Robust Adaptive Kalman Filter against Sensor/Actuator Faults

CHINGIZ HAJIYEV
Department of Aeronautical Engineering,
Istanbul Gelisim University,
Istanbul,
TURKEY

Abstract: - A new fault-tolerant estimating approach for unmanned aerial vehicle (UAV) dynamics in the presence of sensor/actuator faults is proposed, which is both adaptive and robust. This study discusses how to choose between adaptive and robust approaches when a sensor or actuator fails. We provide an adaptive method with Q-adaptation as well as a robust method with R-adaptation. The Kalman filter detects faults using the chi-square distribution of the normalized quadratic innovation function (NQI). After detecting a fault, it is recommended to run both R-adaptive and Q-adaptive Kalman filters concurrently and compare their estimation capabilities to distinguish between sensor and actuator faults. As a performance criterion, the mean-squared residuals between estimation and extrapolation values of robust and adaptive filters are proposed.

Key Words:- Robust Adaptive Kalman Filter, R-adaptation, Q-adaptation, Unmanned Aerial Vehicle, sensor fault, actuator fault, normalized innovation.

Received: September 9, 2025. Revised: April 11, 2026. Accepted: May 5, 2026. Published: July 7, 2026.

1 Introduction

Detection and isolation of sensor/actuator faults in aircraft control systems can be accomplished using model-based Fault Detection and Isolation (FDI) methods, [1], [2], [3], [4], [5], [6], [7].

The study [6] describes a method for detecting and isolating aircraft sensor and control surface/actuator faults that affect the Kalman filter's innovation sequence mean. The Extended Kalman Filter (EKF) is constructed to estimate the nonlinear flight dynamics of an F-16 fighter, and the effects of sensor and actuator faults in the EKF's innovation sequence are investigated. An algorithm based on the Doyle-Stein condition allows for fault isolation, making it easier to discriminate between actuator and sensor problems. In [6], a robust KF insensitive to actuator faults is described as one that meets the Doyle-Stein criterion.
In [7], an effective strategy for isolating sensor and actuator faults that affect the Kalman filter's innovation sequence is presented and used on a dynamics-based UAV model. To determine if the problem is with the sensor or the actuator, a linear adaptive two-stage Kalman filter (TSKF) is developed that is unaffected by actuator faults.

The study [8] presents a fault detection technique for sensor/actuator fault detection. This method uses an embedded Kalman filter to update the weight on the parameters of a neural network used for fault detection. Using MATLAB SIMULINK, the proposed technique has been evaluated on the WVUYF-22 small UAV model. The results of the simulation demonstrate that the proposed approach is capable of effectively detecting and identifying different types of faults that occur in UAV actuators and sensors.

The work [9] uses model-based state estimation methodologies to address sensor, actuator, and component fault detection, identification, and classification in nonlinear helicopter systems. The Extended Kalman Filter based on Interactive Multi-Models and the Unscented Kalman Filter based on Interactive Multi-Models are examined. Statistical measures of residual analysis, stochastic likelihood ratio, and model probability have been proposed to solve the fault detection problem. The algorithm was used on a helicopter with two degrees of freedom, and the results are shown for different fault scenarios. From the results, better fault detection performance was obtained by using the Unscented Kalman Filter based on the Interactive Multi-Model.

The three data-driven statistical residual-based time series approaches for rotor fault detection and identification in multicopters are introduced, examined, and critically evaluated in the study, [10]. The developed methods are based on univariate and multivariate autoregressive representations of multicopter attitudes. Three different levels of turbulence and several rotor fault situations are used to compare the performance of three residual-based statistical fault detection and identification approaches when dealing with external disturbances.

To scale the noise covariance matrix, consider multiplying it by a time-dependent variable. Single fading factor adaptation approaches for process noise covariance correction (Q-adaptation) are discussed in [11], [12]. It is preferable to use a matrix with several fading factors to independently vary the main aspects of the Kalman gain matrix. Instead of using a single component, a matrix consisting of multiple fading components should be used, with the adaptation weighted differently for each parameter. Works [13], [14] show an adaptive estimate of several fading factors in the Kalman filter. Unfortunately, a limitation of these studies, [11], [12], [13], [14] is that they solely examine the Q adaptation process, ignoring the measurement noise covariance correction (R adaptation) strategies.

Furthermore, studies that focus on both the robust R-adaptation and the adaptive Q-adaptation approaches have been published in the literature, [15], [16], [17]. However, these articles do not include a fault isolation scheme and do not explain how to use Robust Adaptive Kalman Filters (RAKF) when sensor/actuator faults occur. These filters can identify whether there is a malfunction or not in the system, but they are unable to identify the type of malfunction.

In this paper, the combined fault isolation and R and Q adaptation methods are solved using a single RAKF that includes the R and Q-adaptation filters. The proposed method does not require an additional fault isolation filter. Following fault detection, it is recommended to run both R-adaptive and Q-adaptive Kalman filters concurrently to distinguish between sensor and actuator faults. The R-adaptation and Q-adaptation processes are compared in terms of estimating performance for fault isolation. It is proposed to use the mean squared residuals between estimation and extrapolation values of the examined filters as an estimation performance criterion. If the actuator fails, the Q adaptation is performed; otherwise, the procedure is completed with the R adaptation.

The paper proceeds as follows. In Section 2, the RAKF algorithm for the UAV state estimation is presented. In Section 3, a sensor/actuator fault isolation technique based on the performance analysis of the R-adaptation and Q-adaptation algorithms is proposed. In Section 4, performances of the Robust and Adaptive KF algorithms are tested and compared for the cases of different sensor and actuator faults. Section 5 gives a summary of the obtained results and concludes the paper.

2 RAKF for UAV State Estimation

2.1 Preliminaries

For the studied estimation problem, we choose to use the combined model for the longitudinal and lateral equations of motion (see Appendix A). As a result, the state vector of the unmanned aerial vehicle (UAV) $x(j)$ to be estimated comprises the $n = 9$ states.

Assume that the white noise random vectors $w(j)$ and $V(j)$ are mutually uncorrelated.

The state vector (A-3) (Appendix-A) can be determined with the linear optimal Kalman filter (OKF), [18]. The **f**ollowing equations represent the OKF's estimation value and gain matrix:

$$\hat{x}(j/j) = \hat{x}(j/j-1) + K(j)\Delta(j) \tag{1}$$

$$K(j) = P(j/j-1)H^T(j)P_\Delta^{-1} \tag{2}$$

where $\hat{x}(j/j-1) = A\hat{x}(j-1/j-1) + Bu(j-1)$ is the extrapolation value, $\Delta(j)$ and $P_\Delta(j)$ what are the innovation and innovation covariance, respectively.

The formulas for the $\Delta(j)$ and $P_\Delta(j)$ are:

$$\Delta(j) = z(j) - H(j)\hat{x}(j/j-1) \tag{3}$$

$$P_\Delta(j) = H(j)P(j/j-1)H(j) + R(j) \tag{4}$$

where

$$P(j/j-1) = AP(j-1/j-1)A^T + GQ(j-1)G^T \tag{5}$$

Is the covariance matrix of the extrapolation error, $Q(j-1)$ is the covariance matrix of system noise, and $R(j)$ is the covariance matrix of measurement noise.

Accurate UAV state estimates can be obtained using LKF if the system is not faulty. However, if a sensor or actuator fault occurs, the RAKF algorithm should be used instead. In this study, we present the

RAKF algorithm, which combines the R and Q-adaptation approaches.

2.2 RAKF Based on Multiple Measurement Noise Scale Factors

RAKF, based on R-adaptation, can be represented using the measurement noise scaling factors (MNSF). The innovation sample covariance matrix is recommended in this study for fault detection and isolation. The sample covariance matrix for the innovation sequence $\Delta(k)$ is formulated as follows, [19]:

$$\hat{S}_{\Delta}(j) = \frac{1}{M}\sum_{k=j-M+1}^{j} \Delta(k)\Delta^T(k) \tag{6}$$

Here M is the "sliding window" width.

The statistic (6) is proposed to be used for R-adaptation. If the measurements are incorrect due to faults in the estimation system, the Kalman filter equations (1), (2), (3), (4), (5) will give incorrect estimation results. The Kalman innovation sequence is presented for use in determining the scale matrix. To calculate the MNSFs, the real and theoretical values of the innovation covariance matrix can be compared. When a measurement fault arises in the estimation system, the real error surpasses the theoretical error. As a result, a multiple measurement noise scale matrix $S(k)$ is included in the algorithm,

$$\frac{1}{M}\sum_{k=j-M+1}^{j} \Delta(k)\Delta^T(k) = HP(j/j-1)H^T + S(j)R(j)\,, \tag{7}$$

Then, it can be calculated by the expression below:

$$S(j) = \left(\frac{1}{M}\sum_{k=j-M+1}^{j} \Delta(k)\Delta^T(k) - HP(j/j-1)H^T\right)R^{-1}(j) \tag{8}$$

The matrix obtained by the formula (8) may not be diagonal and may contain diagonal elements that are "negative" or less than "one" (which is physically impossible). To avoid this situation, adopt the following guideline while generating the scale matrix, [19]:

$$S^* = diag\left(s_1^*, s_2^*, ..., s_n^*\right), \tag{9}$$

Here

$$s_i^* = \max\left\{1, S_{ii}\right\} \qquad i = 1, n\,. \tag{10}$$

and S_{ii} is the i[th] diagonal element of the matrix S .

In the presence of a measurement fault, $S^*(j)$ it will change and have an impact on the Kalman gain matrix.

$$K(j) = P(j/j-1)H^T\left[HP(j/j-1)H^T + S^*(j)R(j)\right]^{-1} \tag{11}$$

When a sensor fails, the scale matrix element corresponding to the faulty component of the measurement vector increases, resulting in a smaller Kalman gain. As a result, the filter's resistance against sensor fault is ensured, while the fault-induced degradation of the estimation technique is avoided.

2.3 AKF Based on Q-Adaptation

When an actuator fails in the system, the control distribution matrix changes. If an actuator fails, the real uncertainty of the innovation covariance outweighs the theoretical one. Thus, the key idea of Q-adaptation is to determine a suitable matrix of factors for the covariance Q, such that the real and theoretical innovation covariances are equal. As a result, a fading matrix $\Psi(j)$ consisting of several fading coefficients is added to the formula (12) as follows:

$$\begin{aligned}&\frac{1}{M}\sum_{k=j-M+1}^{j} \Delta(k)\Delta^T(k) = \\ &H\left[AP(j-1/j-1)A^T + \Psi(j)GQ(j)G^T\right]H^T + R(j)\end{aligned} \tag{12}$$

Then the fading matrix can be found using the following expression:

$$\begin{aligned}\Psi(j) = H^{-1}&\left[\frac{1}{M}\sum_{k=j-M+1}^{j} \Delta(k)\Delta^T(k) - HAP(j-1/j-1)A^TH^T - R(j)\right] \\ &\times\left(GQ(j)G^TH^T\right)^{-1}\end{aligned} \tag{13}$$

In a specific scenario where all states are measured (as in this case $H = I$), (13) reduces to formula (14)

$$\begin{aligned}\Psi(j) = &\left[\frac{1}{M}\sum_{k=j-M+1}^{j} \Delta(k)\Delta^T(k) - AP(j-1/j-1)A^T - R(j)\right] \\ &\times\left(GQ(j)G^T\right)^{-1}\end{aligned} \tag{14}$$

The resulting fading matrix must be diagonalized, as in the case of the adaptation R, since the matrix Q must be a diagonal, positive definite matrix

$$\Psi^* = diag\left(\phi_1^*, \phi_2^*, ..., \phi_n^*\right). \quad (15)$$

where,

$$\phi_i^* = \max\left\{1, \Psi_{ii}\right\} \quad i = 1, \ldots, n. \quad (16)$$

and Ψ_{ii} represents the i[th] diagonal element of the matrix Ψ. If the system has an actuator fault**,** the fading matrix $\Psi^*(j)$ should be included in the estimation algorithm as,

$$P(j/j-1) = AP(j-1/j-1)A^T + \Psi^*(j)GQ(j)G^T \quad (17)$$

3 Sensor/Actuator FDI

3.1 Sensor/Actuator Fault Detection

The fault detection method is applied by testing the statistical function at each evaluation step. Two hypotheses are presented:

γ_0: Normal system operation.

γ_1: System is faulty.

To detect faults, it is proposed to use the normalized quadratic innovation function (NQI):

$$NQI(j) = \Delta^T(j)\left[HP(j/j-1)H^T + R(j)\right]^{-1}\Delta(j) \ . \quad (18)$$

The statistical function (18) has a χ^2 -distribution with a degree of freedom N (N is the dimension of the innovation vector).

If the significance level, α, is set to,

$$P\left\{\chi^2 > \chi^2_{\alpha,N}\right\} = \alpha; \qquad 0 < \alpha < 1, \quad (19)$$

The threshold $\chi^2_{\alpha,N}$ can be found. If the hypothesis γ_1 is right, the statistic $NQI(k)$ will exceed the threshold value $\chi^2_{\alpha,N}$, i.e.

$$\gamma_0 : NQI(j) \le \chi^2_{\alpha,N} \qquad \forall k$$
$$\gamma_1 : NQI(j) > \chi^2_{\alpha,N} \qquad \exists k \ . \quad (20)$$

3.2 Sensor/Actuator Fault Isolation

In this study, the combined fault isolation and R- and Q-adaptation procedures are solved using a single RAKF including R- and Q-adaptive filters.

When a fault is detected, it is proposed to run R-adaptive and Q-adaptive Kalman filters at the same time to distinguish between sensor and actuator faults.

For fault isolation, it is recommended to compare the estimation performances of the R-adaptation and Q-adaptation processes. The R-adaptation and Q-adaptation methods presented in this research are scaling approaches based on innovation covariance rather than direct matrix estimation. As a result, in the event of a sensor or actuator fault, the gain matrices of both the RKF and AKF algorithms adapt to the change in innovation covariance.

As the estimation performance statistic, it is proposed to pick the square differences between the estimation and extrapolation values of the studied filters after detecting a fault at the iteration τ.

$$\varepsilon(j) = \left[\hat{x}(j/j) - \hat{x}(j/j-1)\right]^T \left[\hat{x}(j/j) - \hat{x}(j/j-1)\right], \quad j \ge \tau \quad (21)$$

In the case of a sensor fault, the R-adaptive KF will perform better (the values of the choosing criterion for the RKF will be lower), but if the actuator fails, the Q-adaptive KF will perform better (the values of the choosing criterion for the RKF will be higher). If the actuator fails, the Q adaptation is performed; otherwise, the procedure is completed with the R-adaptation.

As the estimation performance criterion, it is proposed to select the mean square difference between the estimated and extrapolated values of the filters under study for m implementations after detecting a fault at the iteration τ.

$$\varepsilon^* = \frac{1}{m}\sum_{k=\tau}^{\tau+m}\left[\hat{x}(k/k) - \hat{x}(k/k-1)\right]^T \left[\hat{x}(k/k) - \hat{x}(k/k-1)\right],$$
$$k \ge \tau \quad (22)$$

The performance criterion (22) makes it simple to compare the RKF and AKF performances and reduces the probability of making incorrect decisions.

The algorithm structure depicted in Figure B-1 (Appendix B) summarizes the combined fault isolation, R, and Q adaptation techniques.

4 Simulation Results and Discussions

The proposed RAKF is used to model of dynamics of an experimental platform, the ZAGI UAV.

We call the robust approach with R-adaptation the robust Kalman filter (RKF), and the adaptive method with Q-adaptation the adaptive Kalman filter (AKF).

A mathematical model of UAV flight dynamics is described in Appendix A. The simulations are carried out in 1000 steps over 100 seconds, with 0.1 seconds of sampling time. The algorithms are investigated for two types of measurement fault scenarios (continuous bias at measurements and measurement noise increment) and an actuator fault associated with loss of efficiency. In the event of a sensor/actuator fault, simulations are performed for the RKF and AKF to compare the outcomes of state estimation and performance criterion (22).

For the fault detection method, the threshold value is taken to be 16.9, which follows from the chi-square distribution for a degree of freedom of 9 and a reliability level of 95%.

4.1 Continuous Bias Type Measurement Fault

The continuous bias term is simulated in the interval $300 \le j \le 600$, applied to the pitch angle gyro measurements as follows:

$$z_\theta(j) = z_\theta(j) + V_\theta(j) + 2 \qquad (300 \le j \le 600) \tag{23}$$

The behavior of the performance statistic (21) in the presence of pitch gyroscope bias using the RKF and AKF algorithms is shown in Figure 1 and Figure 2, respectively.

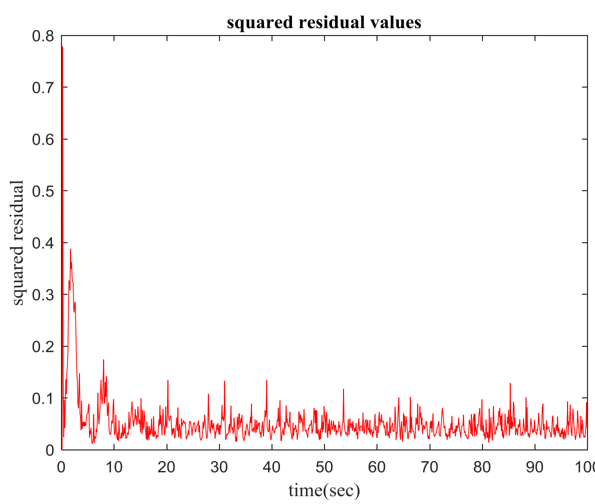

Fig. 1: Performance criterion $\varepsilon(k)$ values for the RKF in the presence of pitch angle gyro bias
Source: Created by the author

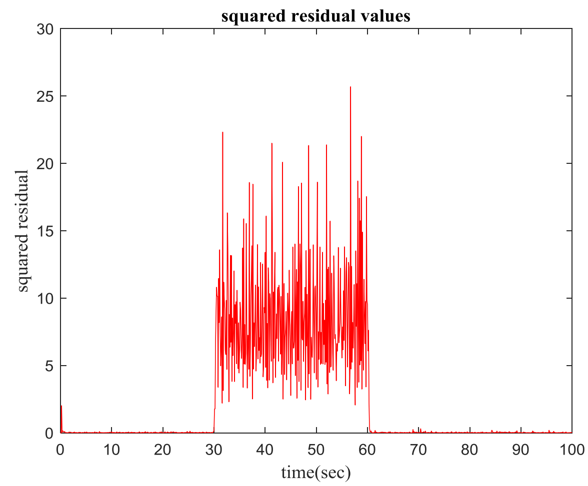

Fig. 2: Behaviour of the performance criterion $\varepsilon(k)$ for the AKF in the presence of pitch angle gyro bias
Source: Created by the author

The values of the performance criterion (22) for the RKF and AKF were obtained $m = 20$, respectively.

$\varepsilon^*_{RKF} = 0{,}0503$ and $\varepsilon^*_{AKF} = 7{,}7804$

As shown $\varepsilon^*_{RKF} << \varepsilon^*_{AKF}$, this inequality corresponds to a sensor fault, and it is advised that the estimating method proceed with the RKF.

Figure 3 and Figure 4 show the pitch angle and forward velocity estimation results of RKF with the pitch angle gyro bias, and Figure 5 and Figure 6 show the similar results obtained with AKF.

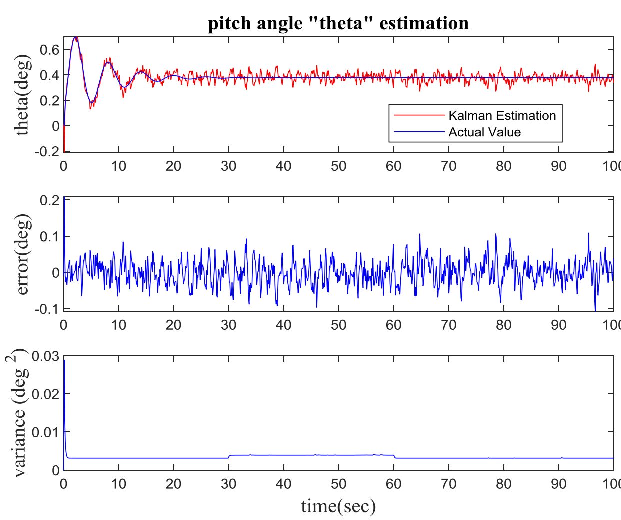

Fig. 3: Estimation result for the pitch angle by the RKF in the presence of pitch angle gyro bias
Source: Created by the author

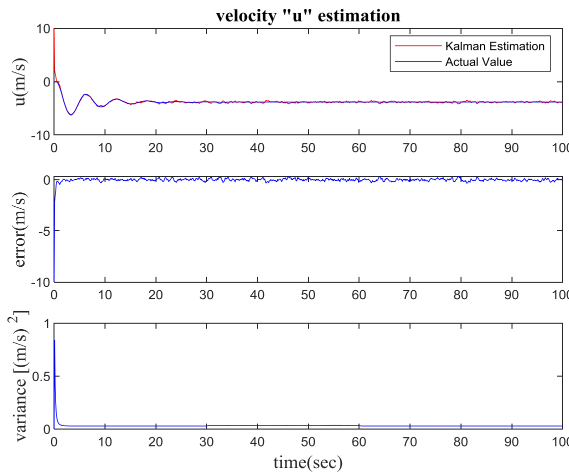

Fig. 4: Estimation result for the forward velocity by the RKF in the presence of pitch angle gyro bias
Source: Created by the author

Figure 3, Figure 4, Figure 5 and Figure 6 demonstrate that the RKF outperforms the AKF in the presence of pitch angle gyro bias. The RKF ensures accurate estimation results for the entire interval, whereas the AKF fails under pitch angle gyro fault situations.

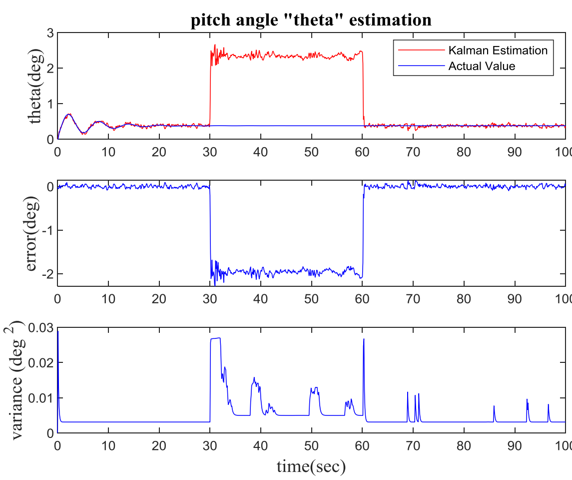

Fig. 5: Estimation result for the pitch angle by the AKF in the presence of pitch angle gyro bias
Source: Created by the author

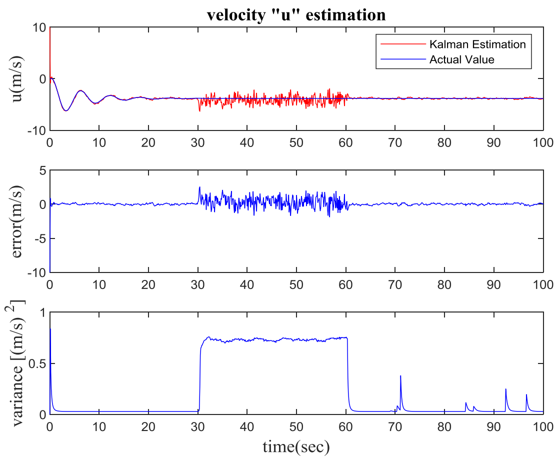

Fig. 6: Estimation result for the forward velocity by the AKF in the presence of pitch angle gyro bias
Source: Created by the author

4.2 Noise Increment Type Measurement Fault

The noise increment type measurement fault is simulated in the interval $300 \le j \le 600$, applied to the pitch angle gyro measurements as follows:

$$z_\theta(j) = z_\theta(j) + V_\theta(j) \times 10, \qquad (300 \le j \le 600). \tag{24}$$

The performance statistic (21) graphs for the RKF and AKF algorithms are given in Figure 7 and Figure 8, respectively.

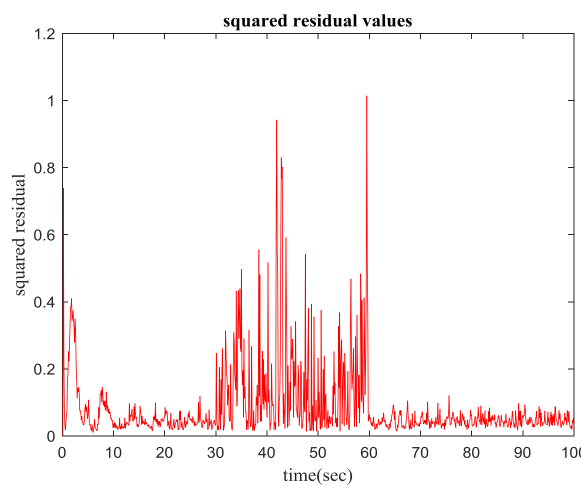

Fig. 7: Performance criterion $\varepsilon(k)$ values for the RKF in the presence of pitch angle gyro noise increment
Source: Created by the author

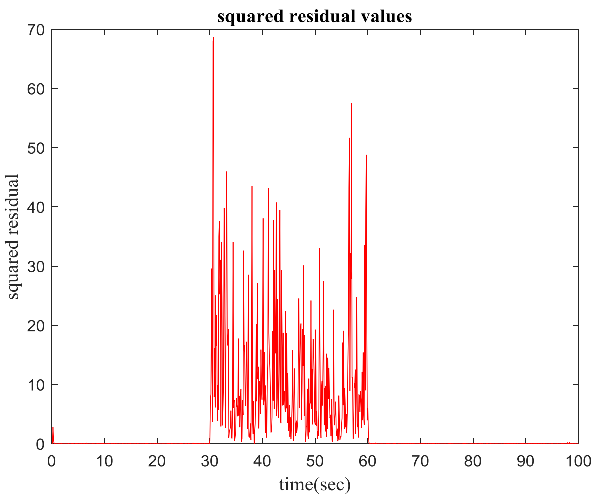

Fig.8: Performance criterion $\varepsilon(k)$ values for the AKF in the presence of pitch angle gyro noise increment
Source: Created by the author

As shown in Figure 7 and Figure 8, in the situation of pitch angle gyro noise increment, RKF performance statistic values (21) are much lower than AKF.

For $m = 20$ the performance criterion values (22) for RKF and AKF are determined as follows:

$$\varepsilon^*_{RKF} = 0{,}0871 \qquad \text{and} \qquad \varepsilon^*_{AKF} = 19{,}2337$$

As can be seen $\varepsilon^*_{RKF} < \varepsilon^*_{AKF}$, the sensor fault has been detected in the system. In this situation, the estimation procedure should be resumed using RKF. Figure 9 and Figure 10 show the results of the RKF pitch angle and forward velocity estimation with the pitch angle gyro noise increment, and Figure 11 and Figure 12 show similar results calculated using AKF.

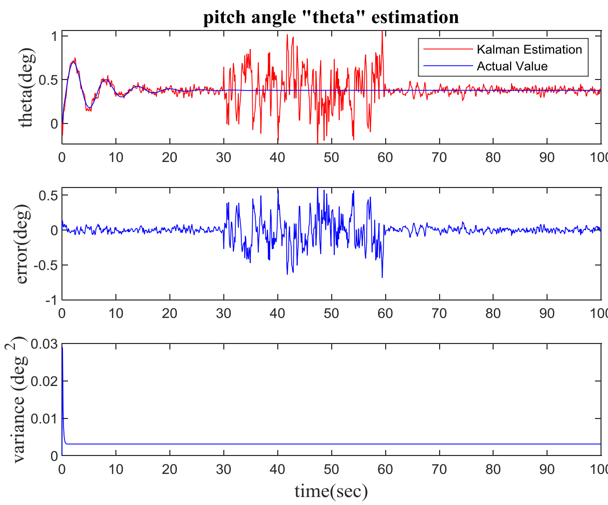

Fig. 9: Estimation result for the pitch angle by the RKF in the presence of pitch angle gyro noise increment
Source: Created by the author

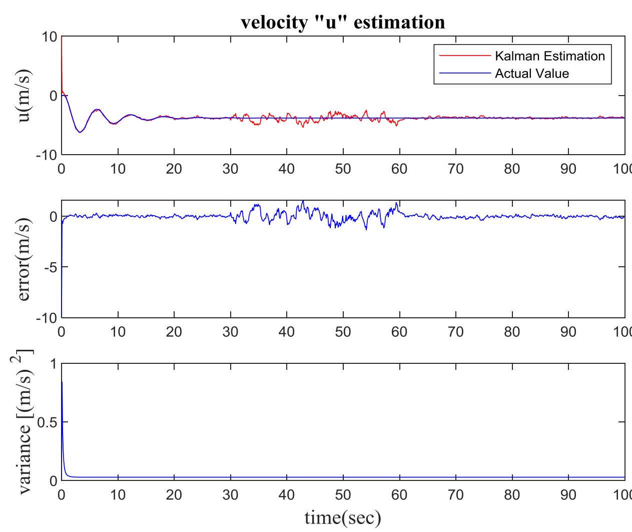

Fig. 10: Estimation result for the forward velocity by the RKF in the presence of pitch angle gyro noise increment
Source: Created by the author

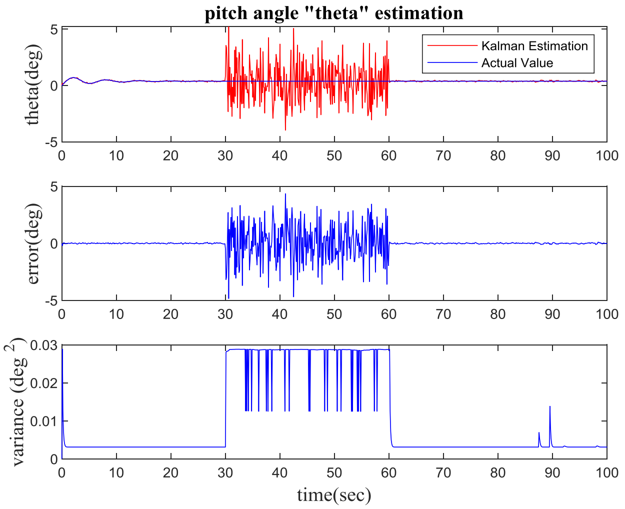

Fig. 11: Estimation result for the pitch angle by the AKF in the presence of pitch angle gyro noise increment
Source: Created by the author

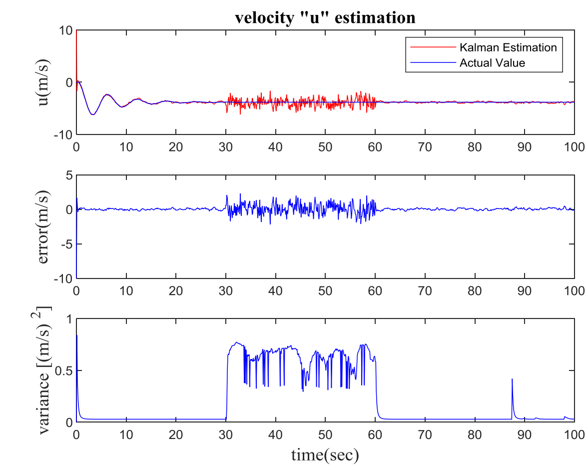

Fig. 12: Estimation result for the forward velocity by the AKF in the presence of pitch angle gyro noise increment
Source: Created by the author

As shown in Figure 8, Figure 9, Figure 10, Figure 11 and Figure 12, in the presence of pitch angle gyro noise increment, the RKF estimation results outperform the AKF results.

4.3 Loss of Effectiveness Type Actuator Fault

In simulations, the actuator fault is represented in the interval $300 \le j \le 600$ by multiplying the first column components of the UAV control distribution matrix by 0.001. This fault corresponds to the loss of elevator effectiveness.

The behaviour of the performance statistics (21) for the RKF and AKF algorithms is shown in Figure 13 and Figure 14, respectively.

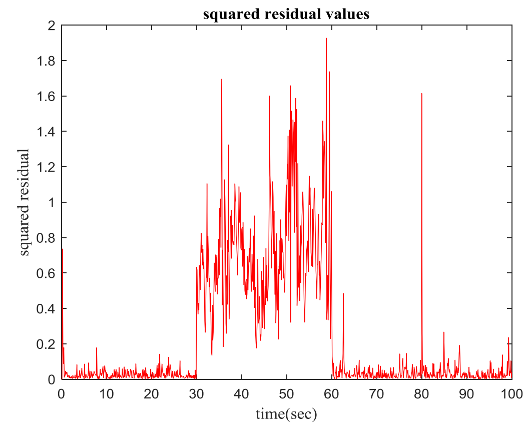

Fig. 13: Performance criterion $\varepsilon(k)$ values for the RKF in the presence of an actuator fault
Source: Created by the author

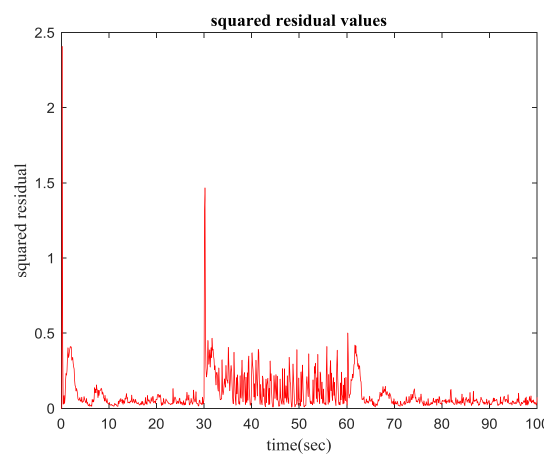

Fig. 14: Performance criterion $\varepsilon(k)$ values for the AKF in the presence of an actuator fault
Source: Created by the author

The simulation findings reveal that in the case of an actuator fault, RKF performance statistic values ε are greater than AKF.

The performance criterion values (22) for RKF and AKF were determined as follows $m = 20$:

$$\varepsilon^*_{RKF} = 0{,}5583 \quad \text{and} \quad \varepsilon^*_{AKF} = 0{,}0762$$

As is obvious $\varepsilon^*_{AKF} < \varepsilon^*_{RKF}$, this inequality relates to an actuator fault in the system, and it is advised that the estimating method proceed with the AKF.

Figure 15 and Figure 16 show the pitch angle and vertical velocity estimation results for RKF in the presence of elevator loss of effectiveness, and Figure 17 and Figure 18 show similar results calculated using AKF.

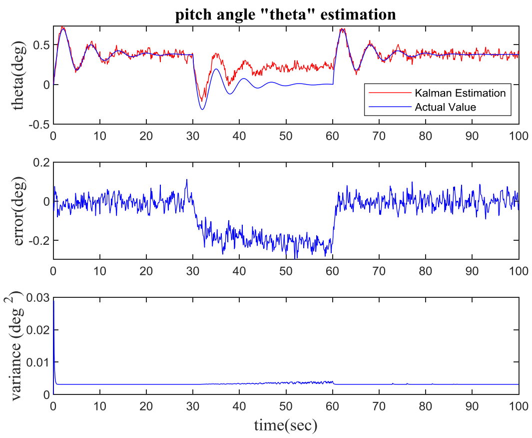

Fig. 15: Estimation result for the pitch angle by the RKF in the presence of an actuator fault
Source: Created by the author

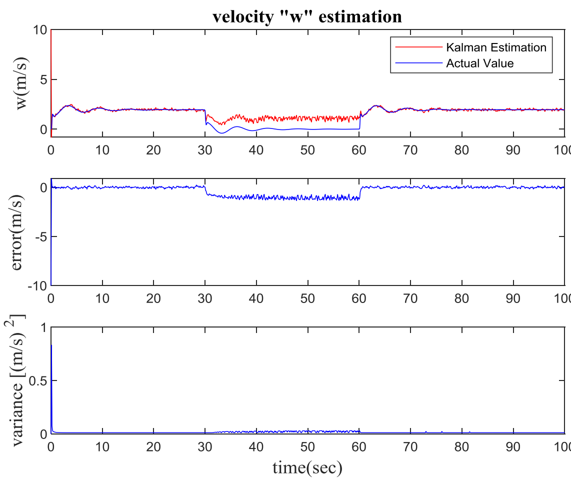

Fig. 16: Estimation result for the vertical velocity by the RKF in the presence of an actuator fault
Source: Created by the author

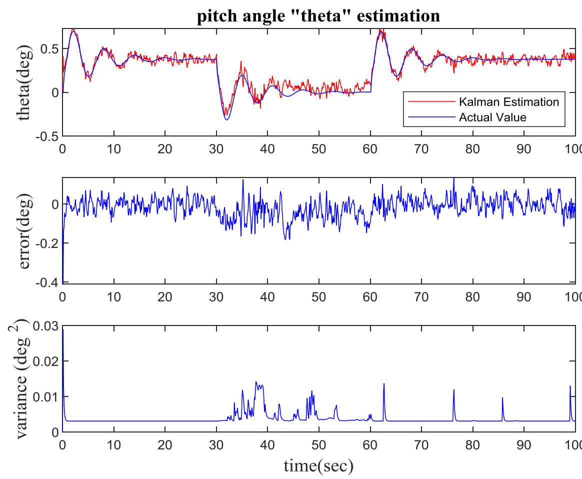

Fig. 17: Estimation result for the pitch angle by the AKF in the presence of an actuator fault
Source: Created by the author

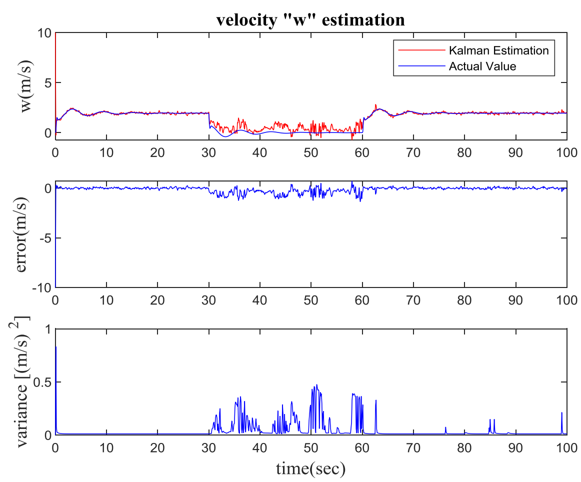

Fig. 18: Estimation result for the vertical velocity by the AKF in the presence of an actuator fault
Source: Created by the author

As shown in Figure 15, Figure 16, Figure 17 and Figure 18, the AKF outperforms the RKF in the presence of an actuator fault.

It is advised that the number of realizations m used to calculate the performance criterion values (22) be chosen from the interval $10 \le m \le 30$.

5 Conclusion

Two opposing techniques are presented in the event of sensor/actuator faults in the system. One is the adaptive approach with a fading factor, which can be insensitive to actuator faults (AKF). The other is a robust method that can be insensitive to measurement faults (RKF). A unique adaptation technique is proposed that allows for a choice between R-adaptation and Q-adaptation procedures. Following fault identification, the unique method proposes running both R-adaptive and Q-adaptive Kalman filters simultaneously and comparing their estimation capabilities to distinguish between sensor and actuator faults.

The mean square differences between estimation and extrapolation values of the investigated filters are used to calculate the estimation performance criterion index. When a sensor fails, the RKF performs better in estimating, but when an actuator fails, the AKF performs better (in terms of the selection criterion). If the actuator fails, the Q adaptation is performed; otherwise, the procedure is completed with the R adaptation.

In this study, the combined fault isolation and R and Q adaptation methods are solved using a single RAKF that includes the R and Q-adaptation filters. The proposed method does not require an additional fault isolation filter. The proposed RAKF is used to model the dynamics of an experimental platform, ZAGI UAV. The holding simulations support the validity of the theoretical results.

References:

[1] P. S. Maybeck, "Multiple model adaptive algorithms for detecting and compensating sensor and actuator/surface failures in aircraft flight control systems," *International Journal of Robust and Nonlinear Control*, Vol. 9, No.14, 1999, pp.1051-1070. https://doi.org/10.1002/(SICI)1099-1239(19991215)9:14<1051: :AID-RNC452>3.0.CO;2-0.

[2] M. H. Amoozgar, Y. M. Zhang, J. Lee, and A. Ng, "A fault detection and diagnosis technique for spacecraft in formation flying. *Preprints of the 8th IFAC Symposium on Fault Detection, Supervision and Safety of Technical Processes (SAFEPROCESS),* August 2012. Mexico City, Mexico, pp.301-306. https://doi.org/10.3182/20120829-3-MX-2028.00269.

[3] R. K. Mehra, "On the identification of variance and adaptive Kalman filtering," *IEEE Transactions on Automatic Control*, Vol. 15, 1970, pp. 175-184. DOI: 10.1109/TAC.1970.1099422.

[4] A. H. Mohamed, K. P. Schwarz, "Adaptive Kalman filter for INS/GPS," *Journal of Geodesy*, Vol. 73, 1999, pp. 193-203. https://doi.org/10.1007/s001900050236.

[5] J. Wang, M. P. Stewart, M. Tsakiri, "Adaptive Kalman filtering for integration of GPS with GLONASS and INS," in: *Proceedings of the 1999 International Geodesy Symposia (IUGG 99),* Birmingham, UK, 1999. https://doi.org/10.1007/978-3-642-59742-8_53.

[6] C. Hajiyev, F. Caliskan, "Sensor and control surface/actuator failure detection and isolation applied to F-16 flight dynamics," *Aircraft Engineering and Aerospace Technology*, Vol. 77, 2005, pp.152-160. https://doi.org/10.1108/00022660510585992.

[7] F. Caliskan, C. Hacizade, "Sensor and actuator FDI applied to an UAV dynamic model. *Preprints of the 19th World Congress, The International Federation of Automatic Control*, Cape Town, South Africa. August, 2014, pp. 12220-12225. https://doi.org/10.3182/20140824-6-ZA1003.01013.

[8] A. Abbaspour, P. Aboutalebi, K. K. Yen, A. Sargolzaei, "Neural adaptive observer-based sensor and actuator fault detection in nonlinear systems: Application in UAV," *ISA Transactions*, Vol. 67, 2017, pp. 317–329. https://doi.org/10.1016/j.isatra.2016.11.005.

[9] M. Raghappriya and S. Kanthalakshmi, "Non-linear model-based stochastic fault diagnosis of 2 DoF helicopter," *Control Engineering and Applied Informatics,* Vol 22, No. 3, 2020, pp. 62-73. ISSN: 1454-8658.

[10] A. Dutta, M. McKay, F. Kopsaftopoulos, F. Gandhi, Statistical residual-based time series methods for multicopter fault detection and identification," *Aerospace Science and Technology,* Vol. 112, 2021, 106649. DOI: 10.1016/j.ast.2021.106649.

[11] C. Hu, W. Chen, Y. Chen. and D. Liu, "Adaptive Kalman filtering for vehicle navigation," *Journal of Global Positioning Systems*, Vol. 2, 2003, pp. 42-47. ISSN*: 1446-3156.*

[12] W. Ding, J. Wang, C. Rizos, "Improving adaptive Kalman estimation in GPS/INS integration," *The Journal of Navigation*, Vol 60, 2007, pp. 517–529. DOI: 10.1017/S0373463307004316.

[13] Y. Geng, J. Wang, "Adaptive estimation of multiple fading factors in Kalman filter for navigation applications," GPS Solutions, Vol. 12, 2008, pp. 273-279. https://doi.org/10.1007/s10291-007-0084-6.

[14] H. E. Soken and Ch. Hajiyev. Adaptive fading UKF with Q-adaptation: application to pico satellite attitude estimation," *Journal of Aerospace Engineering*, Vol 26, Issue 3, 2013, pp. 628–636. DOI: 10.1061/(ASCE)AS.1943-5525.0000178.

[15] D. J. Jwo, T. P. Weng, "An adaptive sensor fusion method with applications in integrated navigation," *The Journal of Navigation*, Vol. 61, 2008, pp. 705–721. DOI: 10.1017/ S0373463308004827.

[16] D. J. Jwo, S. C. Chang, "Particle swarm optimization for GPS navigation Kalman filter," *Aircraft Engineering and Aerospace Technology: An International Journal*, Vol. 81, 2009, pp.343-352. DOI: 10.1108/00022660910967336.

[17] K. H. Kim, J. G. Lee, C. G. Park, "Adaptive two-stage Kalman filter in the presence of unknown random bias," *International Journal of Adaptive Control and Signal Processing*, Vol. 20, 2006, pp.305-319. DOI: 10.1002/acs 900.

[18] R. E. Kalman, "A new approach to linear filtering and prediction problems," *ASME Journal of Basic Engineering,* Vol. 82, 1960, pp. 35-45. https://doi.org/10.1115/1.3662552.

[19] C.Hajiyev, "Adaptive filtering against sensor/actuator faults," *12th IFAC Symposium on Fault Detection, Supervision on Fault Detection, Supervision and Safety for Technical Processes (SAFEPROCESS*- 2024), Ferrara, Italy, June 2024. IFAC PapersOnline, Vol. 58, Iss 4, 2024, pp. 336–341. https://doi.org/10.1016/j.ifacol.2024.07.240.

[20] J. S. Matthews, "Adaptive Control of Micro Air Vehicles," M.Sc. Thesis, Department of Electrical and Computer Engineering, Brigham Young University, Utah, USA, 2006. https://scholarsarchive.byu.edu/etd/756

Contribution of Individual Authors to the Creation of a Scientific Article (Ghostwriting Policy)

The author contributed to the present research at all stages from the formulation of the problem to the final findings and solution.

Sources of Funding for Research Presented in a Scientific Article or the Scientific Article Itself

No funding was received for conducting this study.

Conflict of Interest

The authors have no conflicts of interest to declare.

APPENDIX-A

Mathematical Model of UAV Movement

The equations of UAV motion are studied in two stages: longitudinal and lateral. The linearized longitudinal equation in state space form is [20]:

$$x^{lon}(j+1) = A^{lon}x^{lon}(j) + B^{lon}u^{lon}(j) + G^{lon}w^{lon}(j) \qquad \text{(A-1)}$$

where

$$x^{lon}(j) = \begin{bmatrix}\Delta u & \Delta w & \Delta q & \Delta\theta & \Delta h\end{bmatrix}_j^T;$$

$$A^{lon} = \begin{bmatrix} X_u & X_w & 0 & -g & 0 \\ Z_u & Z_w & u_0 & 0 & 0 \\ M_u + M_{\dot w}Z_u & M_w + M_{\dot w}Z_w & M_q + M_w u_0 & 0 & 0 \\ 0 & 0 & 1 & 0 & 0 \\ 0 & -1 & 0 & u_0 & 0 \end{bmatrix};$$

$$B^{lon} = \begin{bmatrix} X_{\delta e} & X_{\delta T} \\ Z_{\delta e} & Z_{\delta T} \\ M_{\delta e} + M_{\dot w}Z_{\delta e} & M_{\delta T} + M_{\dot w}Z_{\delta T} \\ 0 & 0 \\ 0 & 0 \end{bmatrix}; u^{lon}(j) = \begin{bmatrix}\Delta\delta_e \\ \Delta\delta_T\end{bmatrix}_j.$$

G^{lon} is the 5×5 transition matrix of longitudinal system noise; $w^{lon}(j)$ is the Gaussian white longitudinal system noise, $\Delta(.)$ refers to the perturbed condition, Δu is the forward velocity, Δw is the vertical velocity, $\Delta\theta$ is the pitch angle, Δq is the pitch rate, and Δh is the height.

The linearized equations of lateral motion of the UAV can be written as follows [20],

$$x^{lat}(j+1) = A^{lat}x^{lat}(j) + B^{lat}u^{lat}(j) + G^{lat}w^{lat}(j) \qquad \text{(A-2)}$$

where

$$x^{lat}(j) = \begin{bmatrix}\Delta\beta & \Delta p & \Delta r & \Delta\phi\end{bmatrix}_j^T;$$

G^{lat} Is the 4×4 transition matrix of lateral system noise; $w^{lat}(j)$ is the Gaussian white lateral system noise, $\Delta\beta$ is the sideslip angle, Δp is the roll rate, Δr is the yaw rate, and $\Delta\phi$ is the roll angle.

$$A^{lat} = \begin{bmatrix} \frac{Y_\beta}{u_0} & \frac{Y_p}{u_0} & -\frac{u_0 - Y_r}{u_0} & \frac{g\cos(\theta_0)}{u_0} \\ L_\beta & L_p & L_r & 0 \\ N_\beta & N_p & N_r & 0 \\ 0 & 1 & 0 & 0 \end{bmatrix};$$

$$B^{lat} = \begin{bmatrix} 0 & \frac{Y_{\delta r}}{u_0} \\ L_{\delta a} & L_{\delta r} \\ N_{\delta a} & N_{\delta r} \\ 0 & 0 \end{bmatrix}; u^{lat}(j) = \begin{bmatrix}\Delta\delta_a \\ \Delta\delta_r\end{bmatrix}_j.$$

The notations of the parameters entering Equations (A-1) and (A-2) can be found in [20].
By combining Eq. (A-1) and Eq. (A-2), we have

$$\begin{aligned} x(j+1) &= Ax(j) + Bu(j) + Gw(j) \\ z(j+1) &= Hx(j+1) + V(j+1) \end{aligned} \qquad \text{(A-3)}$$

where

$$x(j) = \begin{bmatrix}\Delta u & \Delta w & \Delta q & \Delta\theta & \Delta h & \Delta\beta & \Delta p & \Delta r & \Delta\phi\end{bmatrix}_j^T$$

$$, u(j) = \begin{bmatrix}\Delta\delta_e & \Delta\delta_T & \Delta\delta_a & \Delta\delta_r\end{bmatrix}_j^T$$

$$A = \begin{bmatrix} A^{lon} & 0 \\ 0 & A^{lat} \end{bmatrix}, B = \begin{bmatrix} B^{lon} & 0 \\ 0 & B^{lat} \end{bmatrix}$$

$V(j+1)$ It is a random 9-dimensional vector of measurement noise, and H is the measurement matrix of the system.

APPENDIX-B
Structure of the Proposed RAKF

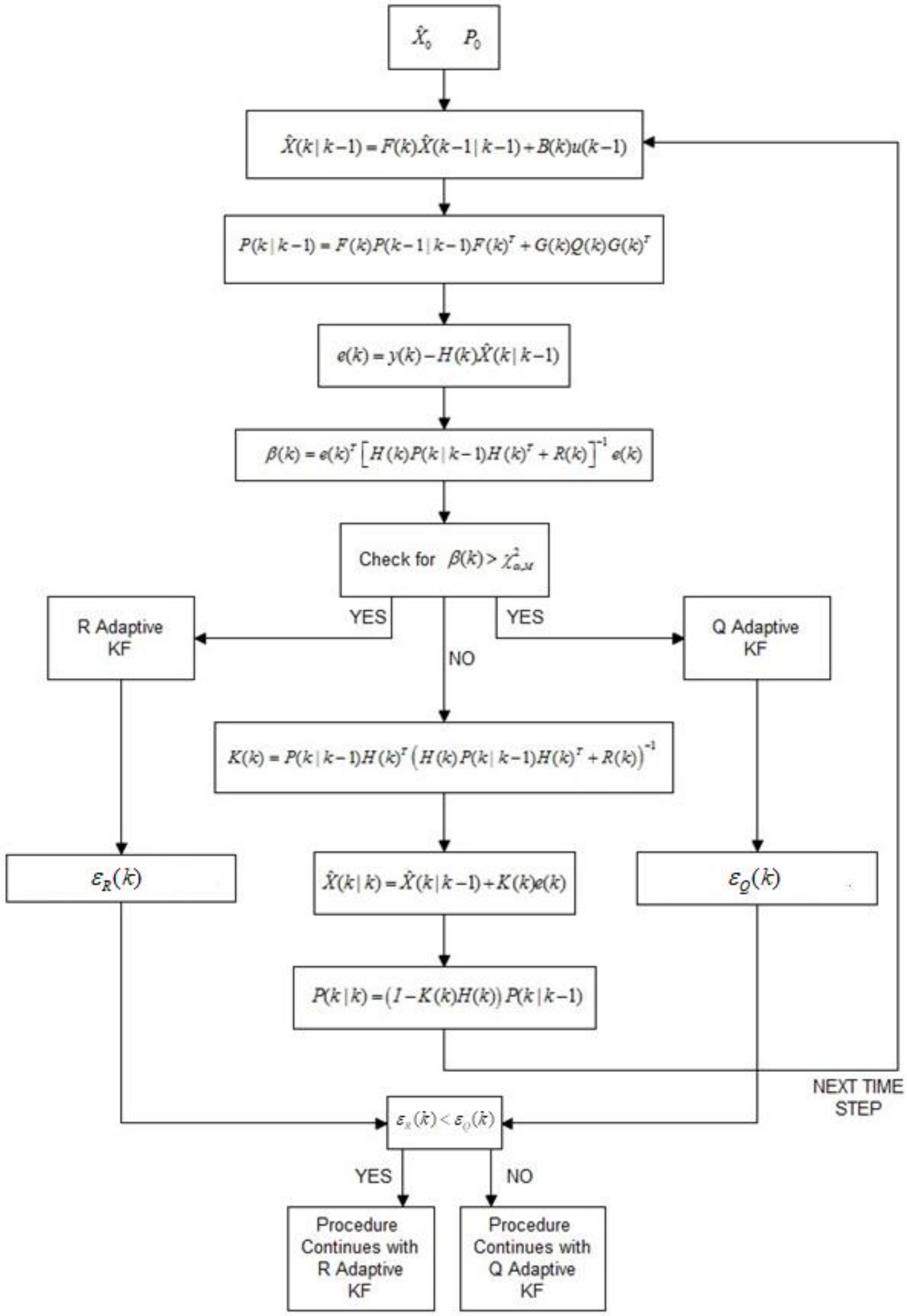

Fig. B-1: Structure of the proposed RAKF against sensor/actuator faults
Source: Created by the author